Computational Study on Space Coiling Acoustic Metamaterial with Resonator for Broadband Low-frequency Noise Control

R Karthik*& K Srinivasan
Department of Mechanical Engineering, Indian Institute of Technology Madras,
Chennai, India - 600036

Abstract

In this study, the proposed Acoustic Metamaterial (AMM) controls low-frequency noise in a wide range. The designed AMM structure is compact andhas both space coiling channels and a resonator. The acoustic band gap and transmission loss of the AMM structure are computed using the COMSOL Multiphysics software. A wave vector in the irreducible Brillouin zone versus frequency is used to plot the acoustic band diagram. As per the Bloch theorem, the result shows that low-frequency broadband noise attenuation occurs within the band gap formation. In this study, three different cases are discussed by varying the thickness (L) of the space coiling structure. The decreasing L acts as a local resonator, and most of the band gap is formed at a high-frequency range. The effect of space coiling structure is dominant with increasing the L value and produces multiple band gaps in a low-frequency regime. These findings suggest a method for designing a lightweight structure to minimize low-frequency noise in future work.

Keywords: Acoustic metamaterial, Low-frequency noise control, Band gap, Transmission loss

1. Introduction

According to mass frequency law, the conventional materials fails to adopt for low frequency broadband noise control with light weight structure. It led to the development of metamaterials. Metamaterial is a material engineered to have properties that are not found in nature, such as negative bulk modulus and mass density. These engineered structures have meta-atoms or unit cells to control and manipulate sound waves. Two decades of research and development on metamaterials have resulted in an effective strategy for alleviating thickness barrier to subwavelength scales and even more profound.[1,2]

In classical literature, many worthwhile efforts have been madeto apply metamaterials for soundproofing applications, which includes micro-perforated panel absorbers[3,4] mass-decorated plates[5,6] meta-surface absorbers[7,8] foam-filled sandwich panels[9,10] and locally resonant structures. Furthermore, Wu et al. [11] studied the local resonance phenomenon of the Helmholtz resonator as a point defect in asonic crystal led to develop a new acoustics devices. Besides, Guenneau et al.[12] theoretically studied that the double 'C' resonators provide negative refraction effect in the low-frequency spectrum. Elford et al.[13] numerically studied the array of sonic crystals.

The FEM model was employed to evaluate the sound transmission properties and band gap formation. They found that the band gap

Corresponding authors: (guru.karthik05@gmail.com)

mostly occurs below the first Bragg frequency. As per the Bloch theorem, band gap formation is the crucial feature for transmission loss in periodic structures.[14] There are various methods developed to evaluate the band structure, such as Multiple Scattering Theory (MST)[15], Plane Wave Expansion Method(PWE) [16], Boundary element method (BEM) [17], and Finite Element Method (FEM).[18] Moreover, Movchan and Guenneau [19] presented an asymptotic analysis of an eigenvalue problem of periodic split-ring resonators. The results show that the model can predict low-frequency stop bands and agree well with FEM.Despite their significant achievements, all these methods have better sound insulation, but only within a small range of frequencies. Multiple resonators were implemented to accomplish broadband noise suppression. Howeveronly the widened initial band gap is observed.Through significant research, scientists have discovered that space coiling structures exhibit various resonances that can result in several bandgaps,thus accommodating more broadband sound insulation. When sound waves move through the channels in these structures, rather than moving straight ahead, their transmission pathways are significantly lengthened producing an ultraslow transmission effect.The high refractive index and other remarkable features, such as negative refraction, acoustic tunneling are made possible by the extension of the transmission route. Liang et al. [20] proposed a 2D space coiling metamaterial. The numerical results demonstrate the negative refraction effect in acoustic tunneling with a near-zero density property. Cheng et al. [21] introduced high-refractive index space coiling AMM for low-frequency noise control applications. Man et al.[22] created the spaced coiling metamaterial to achieve a broad dispersion spectrum. The design produces many bandgaps in higher-order fractal structures. Liu et al. [23] constructed a space coiling metamaterial based on Hilbert fractal AMM to achieve broadband sound insulation. Space-coiling fractal structures have a wide range of applications, such as noise reduction [24], acoustic lenses [25], and broadband acoustic wave filters. [26] In this study, the proposed AMM is based on the combination of local resonance structure with space coiling design. By varying the space coiling structure, three different cases are used for analysis. The acoustic transmission characteristics, eigen-mode analysis, and band gap plot are studied with the help of COMSOL Multiphysics software. The bandgap plot is validated with Plane Wave Expansion (PWE) method.

2. Material and Methods

In the present study a 2D local resonance structure with a space coiling design is considered for the Transmission Loss (TL) characteristics, as shown in Figure 1. This structure's interior resembles the Helmholtz resonator, and the outer structure design, i.e., the wall of the Helmholtz resonator, is adopted from the space coiling structure. In Figure 1, L represents the space coiling structure thickness, t is the wall thickness, and$r_o$and $r_i$are the outer and inner radii, respectively. The design parameters of the considered structures are detailed in Table 1.The Finite Element Method-based COMSOL Multiphysics software is used to study the dispersion phenomenon, eigenmode analysis, and TL characteristics. The computational domain has two parts: steel (white region in Fig 1b) and air (grey region in Fig 1b). The material properties are listed in Table 2.

The Helmholtz equation for the air domain can be expressed as

$$\nabla\left(\frac{1}{\rho}\nabla p\right)+\frac{\omega^2}{\rho c^2}p=0 \qquad (1)$$

Here p is sound pressure, ω is the angular frequency, c and ρ are the speed of sound and density of air medium, respectively. The vibration of the solid part is eliminated because the impedance of the solid domain is moresignificant than air. Further, the solid-acoustic interface is considered as rigid wall boundary condition to simplify the computational model.

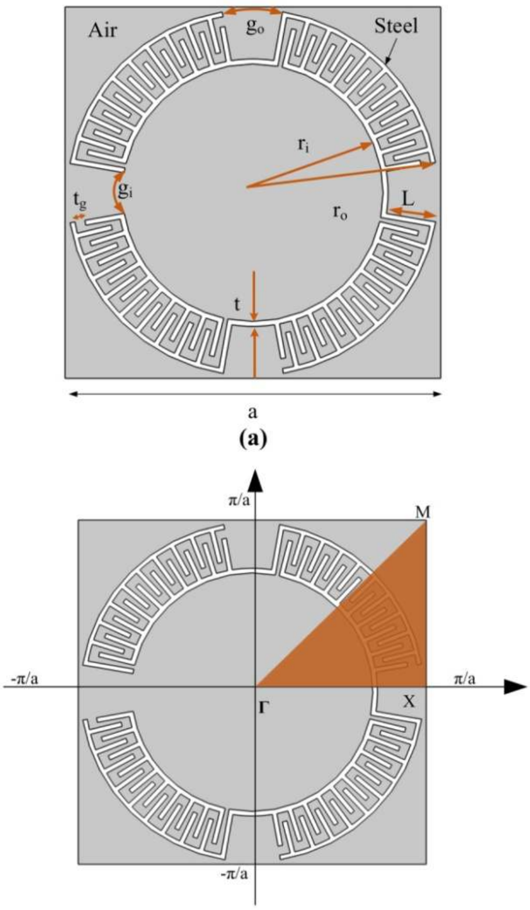

Figure 1: (a) The unit cell with the lattice constant 'a' (b) The Irreducible Brillouin zone of the square lattice

The sound pressure field, as per the Bloch theorem, is expressed in equation(2)

$p(r + a) = p(r)exp(ika)$ (2)

Where r is the position vector and k is Bloch wave-vector. Each unit cell is arranged in a square lattice arrangement with the size of 'a=75mm'. The Floquent Bloch periodic boundary condition is applied to both ends of the boundaries of a unit cell. The band structure is obtained by solving the frequency domain equation with varying $k -$ wave vector in the Irreducible Brillouin zone (IBZ), as shown in Fig 1b.

In real-time, the infinite form of the periodic structure is impossible. Hence, the acoustic performance of the finite periodic structure is evaluated. In this study unit cells are arranged in a 5 × 5 array. As illustrated in Fig 2, the sound waves travel in the x and y directions, and periodic boundary conditions are applied to both sides of the domain. The Perfectly Matched Layer (PML) is employed at both ends of the domain, which helps avoid reflection to the propagation field. The left side of the structure is considered asa Background Pressure Field(BPF). The Transmission loss is calculated as follows:

$$TL = 10\ log_{10} \frac{w_{out}}{w_{in}} \quad (3)$$

$w_{out}$is the transmitted acoustic power measured on the right portion of the structure (green line) and,$w_{in}$is the acoustic power in BPF measured on the left side of the structure (yellow line).

3. Validation

To verify the computational study, the band diagram of the COMSOL result is compared with the Plane Wave Expansion Method (PWE).[27]The simple steel cylinder inclusion in an air medium model is considered for validation. The simulation results perfectly matched the PWE method, as shown in Fig 3a. Using the results of Yu et al.[28] the acoustic characteristic of the computational model is validated.

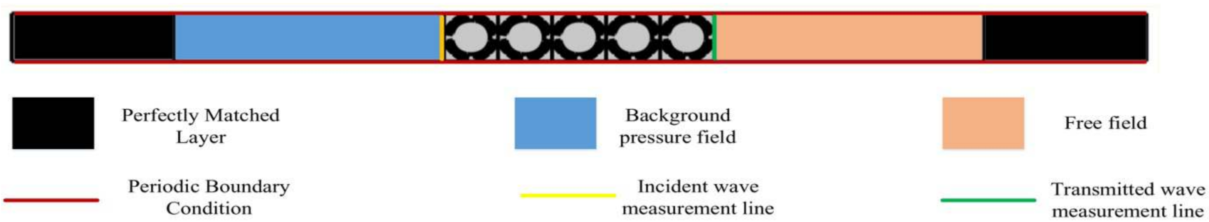

Figure 2: The computational model for transmission loss analysis

4. Results and Discussion

This section discusses computational results on bandgap plots, eigenmode, and transmission loss characteristics of the proposed structure with different incident angles. The band diagram plot and transmission loss plot are shown in Figures 4 (a), 4(b), and 4(c). In case 1, the three different band gaps are observed. Those are 540 to 670 Hz, 684 to 750 Hz, and 800 to 907 Hz, and the cumulative bandwidth is observed to be 250 Hz. Also,in Case 2 three different band gaps are observed, but the width of the last two bands(820-891 Hz & 913-982 Hz) narrowed, and in case 3 a single band gap (560-880 Hz) is observed. Thecumulative bandwidth of case 2 and case 3 are observed to be 340 and 320 Hz, respectively. Therefore, decreasing space coiling thickness' L' reduces the band gap in low frequency. The relative frequency f_R is calculated and is as shown in equation 4. In the three different cases, the f_R values are less than 1, which shows that the designed structure can perform well for subwavelength noise control.

$$f_R = \frac{f_{center}}{f_{reference}} \qquad (4)$$

Here

$$f_{reference} = {}^{c}/_{a}$$

f_{center} - Centre frequency of bandgap, c- speed of sound in m/s and a-lattice constant.

Fig4 shows the transmission loss for three cases studied. A 50 dB TL at 715 Hz is observed for cases 2 & 3.In case 3, only the first band gap is shown in Fig 4; other band gaps are formed in the higher frequency. For case 1, TL is less than 40 dB. Further, with an increasing 'L' value, TL decreases.

The band gap depends on the resolution of eigenfrequencies. The first eigenfrequency for all cases is the same due to external dimension similarity. The second eigenfrequency follows the increasing trend with the decreasing L, as shown in Fig 5

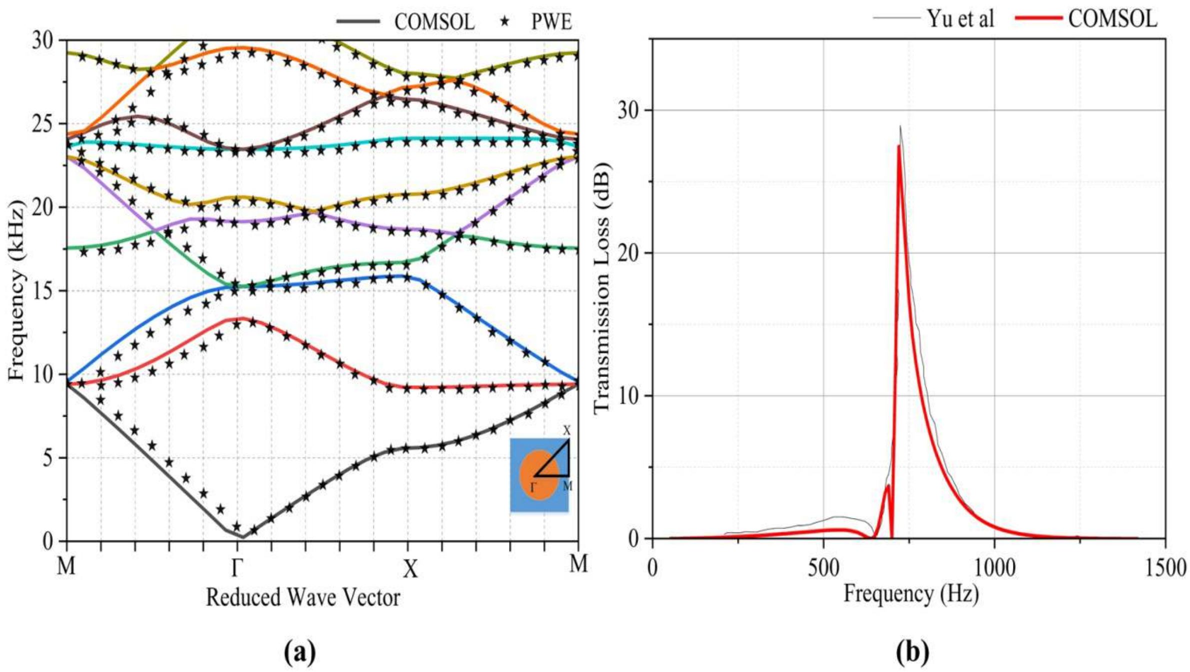

Figure: 3 (a) Validate the COMSOL result with the PWE method (b) Validation of Transmission characteristics of COMSOL result with Yu et al.[28]

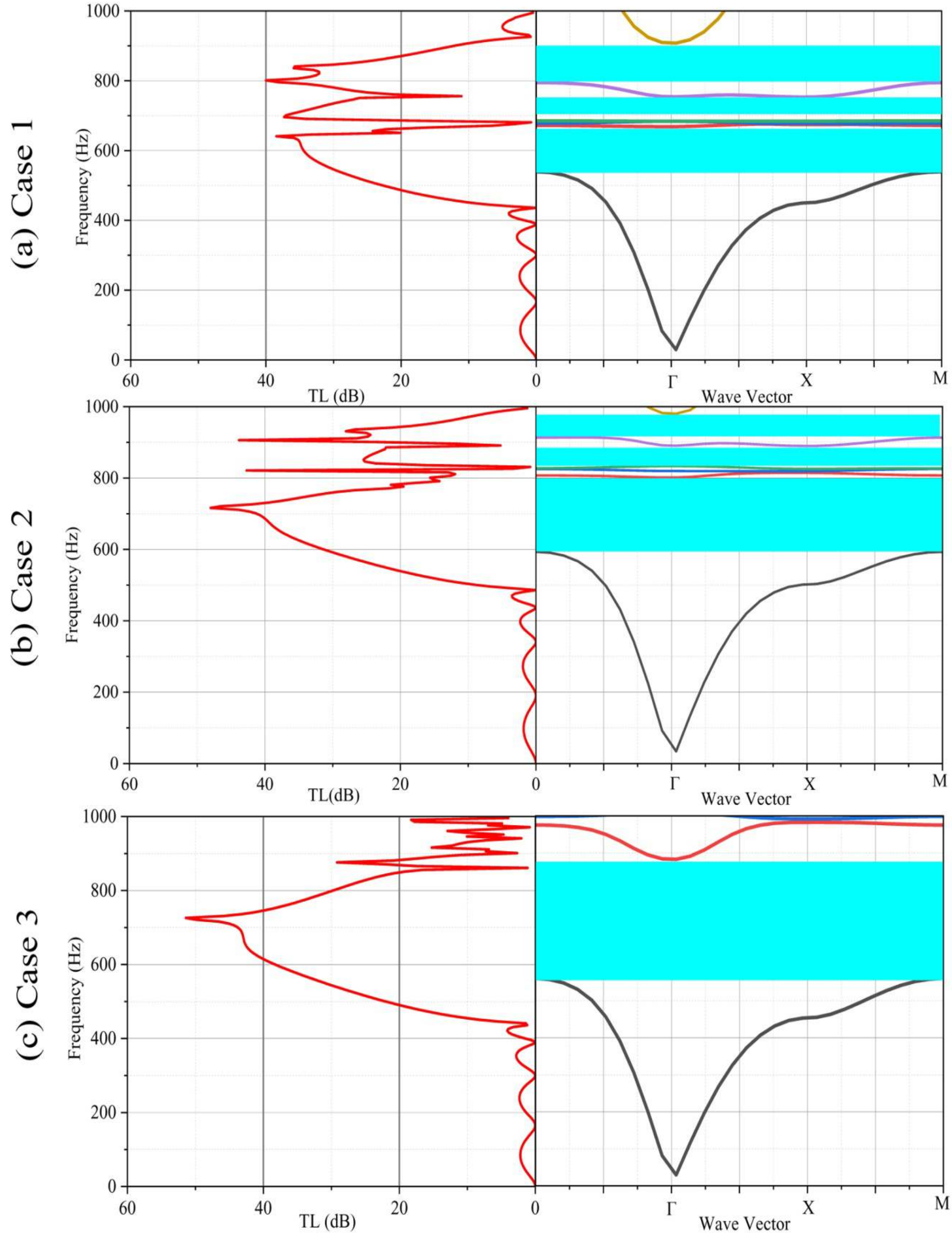

Figure 4: Transmission Loss spectra and band diagram for different cases

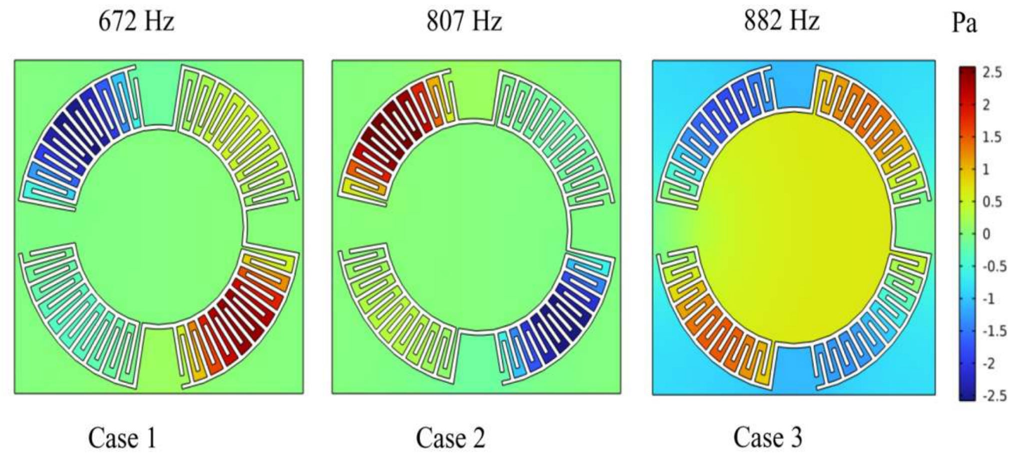

Figure 5: second eigen mode for case1, 2 &3

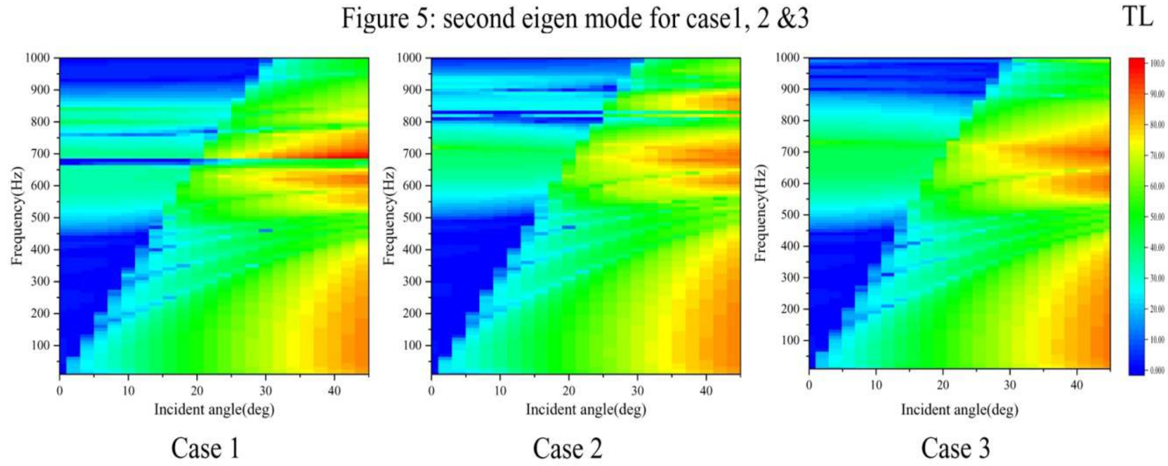

Figure 6: Transmission Loss for different incident angle

.In cases 1 and 2, the resonance effect is created due to the spacecoiling effect. Whereas in case 3, the resonance effect is formed due to the Helmholtz structure. The thickness of the space coiling structure in case 3 is less, thus acting as a local resonance structure. The resonance frequency for case 3 is higher, and a wide range of frequency band gaps is observed. But for cases 1 & 2, several eigen frequencies are formed within 1000Hz, so the number of band gaps also increases due to the space coiling effect.

Therefore for cases 1 & 2, eigen frequencies depend on the space coiling effect due to a higher L value. Meanwhile, case 3 depends on the local resonance effect due to a lower L value.The transmission characteristics of different incident angles are also evaluated. Fig 6 shows that the TL increases when increasing the incident angle and still obey the band gap plot. In case 3, TL is observed for a broader and continuous frequency range of 450-900Hzfor all incident angles. In cases 1 and 2, the TL characteristics are absent in a few frequencies where constructive interference is formed due to the space-coiling resonance.From the Bloch theorem, if the band gaps are wider, it will reduce the broadband noise.To understand the variation of bandgap relation amongdifferent cases, the Total Relative Bandgap (TRB) is expressed as[29].

$$\text{Total Relative Bandgaps} = \sum_{n=1}^{i} \frac{2(f_{u,n}-f_{l,n})}{(f_{u,n}+f_{l,n})} \qquad (6)$$

Where $f_{u,n}$ and $f_{l,n}$ are the upper and lower ends of the bandgap, and i represents the number of bandgaps within the frequency of 1000Hz.

The actual bandwidth and TRB are shown in Fig 7. The decrease in the L value causes the band gap shift to higher frequencies. In case 1, the first bandwidth is only shown here, and others are in the higher frequency range (more than 1000Hz). Multiple bandgaps are formed within the low-frequency region due to the increasing thickness of the space-coiling structure. But the TRB value decreases with increasing the influence of space coiling structure, as shown in Fig 7. These results are promising and can further be improved by optimizing other parameters to make a wider band gap within the low-frequency regime.

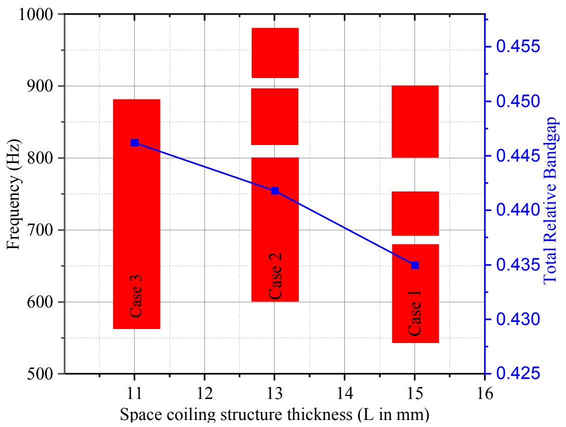

Figure 7: Schematic of band gap and TRB plot

5. Conclusion

The proposed structure based on combine effect of space coiling and local resonance offers a good solution for low-frequency noise control applications. It is found that while increasing the space coiling thickness L, multiple resonance band gaps are formed in the low-frequency region. The eigenfrequency plot shows that case 3 acts as a local resonator at the first band gap due to the lower L value. The simulation result shows cases 2 & 3 have almost 50dB noise attenuation. The TL is calculated for different incident angles, which shows that case 2 have a wider noise attenuation compared to case 1& 3. Therefore the reasonable space coiling thickness provides broadband noise control.

References

[1] Cummer, S. A., Christensen, J. & Alù, A. Controlling sound with acoustic metamaterials. *Nat. Rev. Mater.* **1**, (2016).

[2] Zangeneh-Nejad, F. & Fleury, R. Active times for acoustic metamaterials. *Rev. Phys.* **4**, 100031 (2019).

[3] Park, S. H. Acoustic properties of micro-perforated panel absorbers backed by Helmholtz resonators for the improvement of low-frequency sound absorption. *J. Sound Vib.* **332**, 4895–4911 (2013).

[4] Wu, F. *et al.* Low-frequency sound absorption of hybrid absorber based on micro-perforated panel and coiled-up channels. *Appl. Phys. Lett.* **114**, (2019).

[5] Yang, Z., Mei, J., Yang, M., Chan, N. H. & Sheng, P. Membrane-type acoustic metamaterial with negative dynamic mass. *Phys. Rev. Lett.* **101**, 1–4 (2008).

[6] Huang, T.-Y., Shen, C. & Jing, Y. Membrane- and plate-type acoustic metamaterials. *J. Acoust. Soc. Am.* **139**, 3240–3250 (2016).

[7] Li, J., Wang, W., Xie, Y., Popa, B. I. & Cummer, S. A. A sound absorbing metasurface with coupled resonators. *Appl. Phys. Lett.* **109**, (2016).

[8] Long, H., Shao, C., Liu, C., Cheng, Y. & Liu, X. Broadband near-perfect absorption of low-frequency sound by subwavelength metasurface. *Appl. Phys. Lett.* **115**, (2019).

[9] Wang, D. W. & Ma, L. Sound transmission through composite sandwich plate with pyramidal truss cores. *Compos. Struct.* **164**, 104–117 (2017).

[10] Arunkumar, M. P., Pitchaimani, J., Gangadharan, K. V. & Leninbabu, M. C. Vibro-acoustic response and sound transmission loss

characteristics of truss core sandwich panel filled with foam. *Aerosp. Sci. Technol.***78**, 1–11 (2018).

[11] Wu, L. Y. & Chen, L. W. Wave propagation in a 2D sonic crystal with a Helmholtz resonant defect. *J. Phys. D. Appl. Phys.***43**, (2010).

[12] Guenneau, S., Movchan, A., Pétursson, G. & Ramakrishna, S. A. Acoustic metamaterials for sound focusing and confinement. *New J. Phys.***9**, (2007).

[13] Elford, D. P., Chalmers, L., Kusmartsev, F. V. & Swallowe, G. M. Matryoshka locally resonant sonic crystal. *J. Acoust. Soc. Am.***130**, 2746–2755 (2011).

[14] Bradley, C. E. Time harmonic acoustic Bloch wave propagation in periodic waveguides. Part I. Theory. *J. Acoust. Soc. Am.***96**, 1844–1853 (1994).

[15] Page, J. H. *et al.* Tunneling and dispersion in 3D phononic crystals. *Zeitschrift fur Krist.***220**, 859–870 (2005).

[16] Wu, F., Liu, Z., Liu, Y., Bortot, E. & Shmuel, G. Acoustic band gaps in 2D liquid phononic crystals of rectangular structure Tuning sound with soft dielectrics.

[17] Li, F. L., Wang, Y. S. & Zhang, C. A BEM for band structure and elastic wave transmission analysis of 2D phononic crystals with different interface conditions. *Int. J. Mech. Sci.***144**, 110–117 (2018).

[18] Cselyuszka, N., Se, M. & Crnojević, V. Analysis of Acoustic Metamaterials - Acoustic Scattering Matrix and Extraction of Effective Parameters. *Metamaterials '2012 Sixth Int. Congr. Adv. Electromagn. Mater. Microwaves Opt.* 170–172 (2012).

[19] Movchan, A. B. & Guenneau, S. Split-ring resonators and localized modes. *Phys. Rev. B - Condens. Matter Mater. Phys.***70**, 1–5 (2004).

[20] Liang, Z. & Li, J. Extreme acoustic metamaterial by coiling up space. *Phys. Rev. Lett.***108**, 1–4 (2012).

[21] Cheng, Y. *et al.* Ultra-sparse metasurface for high reflection of low-frequency sound based on artificial Mie resonances. *Nat. Mater.***14**, 1013–1019 (2015).

[22] Man, X. *et al.* Space-coiling fractal metamaterial with multi-bandgaps on subwavelength scale. *J. Sound Vib.***423**, 322–339 (2018).

[23] Liu, Y. *et al.* Fractal Acoustic Metamaterials with Subwavelength and Broadband Sound Insulation. *Shock Vib.***2019**, (2019).

[24] Wen, W. *et al.* Subwavelength Photonic Band Gaps from Planar Fractals. *Phys. Rev. Lett.***89**, 1–4 (2002).

[25] Song, G. Y., Huang, B., Dong, H. Y., Cheng, Q. & Cui, T. J. Broadband Focusing Acoustic Lens Based on Fractal Metamaterials. *Sci. Rep.***6**, 1–7 (2016).

[26] Zhang, P. & To, A. C. Broadband wave filtering of bioinspired hierarchical phononic crystal. *Appl. Phys. Lett.***102**, (2013).

[27] Elford, D. P. Band Gap Formation in Acoustically Resonant Phononic Crystals. 177 (2010).

[28] Yu, X. *et al.* Sound transmission through a periodic acoustic metamaterial grating. *J. Sound Vib.***449**, 140–156 (2019).

[29] Xu, C. *et al.* Study on broadband low-frequency sound insulation of multi-channel resonator acoustic metamaterials. *AIP Adv.***11**, (2021)